An optimized MP2RAGE sequence for studying both brain and cervical spinal cord in a single acquisition at 3T

Arash Forodighasemabadi, Henitsoa Rasoanandrianina, Mohamed Mounir El Mendili, Maxime Guye, Virginie Callot

An optimized MP2RAGE sequence for studying both brain and cervical spinal cord in a single acquisition at 3T.

Authors

Arash Forodighasemabadi[1,2,3,4], Henitsoa Rasoanandrianina[1,2,3,4], Mohamed Mounir El Mendili[1,2], Maxime Guye[1,2], and Virginie Callot[1,2,4,*]

Affiliations

[1] Aix-Marseille Univ, CNRS, CRMBM, Marseille, France

[2] APHM, Hopital Universitaire Timone, CEMEREM, Marseille, France

[3] Aix-Marseille Univ, Université Gustave Eiffel, LBA, Marseille, France

[4] iLab-Spine International Associated Laboratory, Marseille-Montreal, France-Canada

* Corresponding author

Virginie Callot
CRMBM-CEMEREM, Aix-Marseille Université, Hôpital Universitaire Timone
27 bd Jean Moulin
13385 Marseille cedex 05, France
Office: +334 91 38 84 65 | Email: virginie.callot@univ-amu.fr

Declarations of interest: none

Sponsors and Grants

This work was performed within a laboratory member of France Life Imaging network (grant ANR-11-INBS-0006) and was supported by the Institut Carnot Star, the ARSEP Foundation (Fondation pour l'Aide à la Recherche sur la Sclérose en Plaques) and the CNRS (Centre National de la Recherche Scientifique). The project also received funding from the European Union's Horizon 2020 research and innovation program under the Marie Skłodowska-Curie grant agreement No713750, with the financial support of the Regional Council of Provence-Alpes-Côte d'Azur and A*MIDEX (n° ANR-11-IDEX-0001-02), funded by the Investissements d'Avenir project by the French Government, managed by the French National Research Agency (ANR).

Abbreviations

MP2RAGE: Magnetization Prepared 2 Rapid Acquisition Gradient Echo
TI1/TI2: First and second inversion times
α_1/α_2: First and second RAGE flip angles
cSC: Cervical Spinal Cord
MS: Multiple Sclerosis
ALS: Amyotrophic Lateral Sclerosis
CNR: Contrast to Noise Ratio
WM: White Matter
GM: Gray Matter
CSF: Cerebrospinal Fluid
ROI: Region of Interest
SD: Standard Deviation
COV: Coefficient of Variation
CST: Corticospinal Tracts
PST: Posterior Sensory Tracts
LST: Lateral Sensory Tracts
RST: Reticulo/Rubrospinal Tracts
Pr: Protocol
FOV: Field of view
EPI: Echo Planar Imaging
FLASH: Fast Low- Angle Shot
TR: Repetition Time
PAT: Parallel Acquisition Technique

Abstract

Magnetization Prepared 2 Rapid Acquisition Gradient Echo (MP2RAGE) is a T_1 mapping technique that has been used broadly on brain and recently on cervical spinal cord (cSC). The growing interest for combined investigation of brain and SC in numerous pathologies of the central nervous system such as multiple sclerosis (MS), amyotrophic lateral sclerosis (ALS) and traumatic injuries, now brings about the need for optimization with regards to this specific investigation. This implies large spatial coverage with high spatial resolution and short acquisition time, high CNR and low B_1^+ sensitivity, as well as high reproducibility and robust post-processing tools for T_1 quantification in different regions of brain and SC.

In this work, a dedicated protocol (referred to as Pr-BSC) has been optimized for simultaneous brain and cSC T_1 MP2RAGE acquisition at 3T. After computer simulation optimization, the protocol was applied for in vivo validation experiments and compared to previously published state of the art protocols focusing on either the brain (Pr-B) or the cSC (Pr-SC). Reproducibility and in-ROI standard deviations were assessed on healthy volunteers in the perspective of future clinical use.

The mean T_1 values, obtained by the Pr-BSC, in brain white, gray and deep gray matters were: (mean ± in-ROI SD) 792±27 ms, 1339±139 ms and 1136±88 ms, respectively. In cSC, T_1 values for white matter corticospinal, posterior sensory, lateral sensory and rubro/reticulospinal tracts were 902±41 ms, 920±35 ms, 903±46 ms, 891±41 ms, respectively, and 954±32 ms for anterior and intermediate gray matter. The Pr-BSC protocol showed excellent agreement with previously proposed Pr-B on brain and Pr-SC on cSC, with very high inter-scan reproducibility (coefficients of variation of 0.52±0.36% and 1.12±0.62% on brain and cSC, respectively).

This optimized protocol covering both brain and cSC with a sub-millimetric isotropic spatial resolution in one acquisition of less than 8 minutes, opens up great perspectives for clinical applications focusing on degenerative tissue such as encountered in MS and ALS.

Keywords

T_1 mapping, Magnetization Prepared 2 Rapid Acquisition Gradient Echo, Central Nervous System, Brain, Cervical Spinal Cord

1 Introduction

The T_1 relaxation time, also known as spin-lattice relaxation time, is a MR property of the tissue that holds great potential in characterizing alterations such as demyelination, iron deposition or structural changes occurring in pathologies like Multiple Sclerosis (MS) and Parkinson's disease. Consequently, quantitative measurements of T_1 have been used widely to study such pathologies [1]–[5].

There have been several techniques developed for measuring T_1. To date, Spin-Echo Inversion Recovery (SE-IR) remains the gold standard; but it is not very practical for clinical use because of its long acquisition time [6]. The variant of Inversion Recovery with EPI (IR-EPI) [7] and Look Locker technique with EPI readout [8] are much faster, but they could suffer from geometrical distortions caused by the static magnetic field inhomogeneities, especially when covering a large field of view [9]. Other techniques proposed to date include the variable flip angle (VFA) [10] techniques which are relatively fast and can acquire 3D T_1 maps in clinically feasible times, but the conventional VFA T_1 quantitative mapping could be biased by imperfect spoiling of the transverse magnetization [11].

Meanwhile, the Magnetization Prepared 2 Rapid Acquisition Gradient Echo (MP2RAGE), which is an IR-based technique that acquires two RAGE volumes from which a uniform (UNI) image is derived and used to estimate the T_1 of the tissue, has been proposed [12]. The technique has already been largely used in brain at 3T [13], [14] and 7T [15], [16] to study pathologies like MS and it has shown to be effective in investigating the progression of disease as compared to gold-standard sequences like DIR (Double Inversion Recovery) [17], [18] and FLAIR (Fluid Attenuated Inversion Recovery) [19]. MP2RAGE was also used to study the whole cervical spinal cord (cSC), first at 7T [20] and more recently at 3T [21], [22].

Concurrently, there has been a growing interest in studying the whole central nervous system (CNS) in recent years. Indeed, investigating both brain and SC holds great potential in further understanding pathophysiological relationships occurring in degenerative or traumatic pathologies [23]–[27]. However, the large FOV required to capture the whole brain and cSC and the high sub-millimetric resolution needed to investigate small structures of SC, combined with B_0 inhomogeneities and various artifacts and potential distortions, turn simultaneous brain and cSC imaging into a challenge.

The MP2RAGE technique was previously optimized for brain investigation at 3T [13] and 7T [28] based on CNR and limitation of B_1^+ sensitivity, hence providing "standard protocols" for brain applications. More recently, Rasoanandrianina et al. considered the T_1 values observed on cervical SC GM and WM and proposed a protocol for imaging cervical SC specifically[21]. Since the tissue constraints are not the same for brain and cSC, these protocols are not necessarily optimal to be used in simultaneous brain and cSC imaging.

The present work consequently focuses on an MP2RAGE protocol dedicated to both brain and cSC by considering and examining a wider range of T_1s observed in CNS. Optimization was performed through computer simulation for a higher contrast-to-noise ratio (CNR) while limiting B_1^+ sensitivity. An automatic post-processing pipeline was additionally proposed to quantify T_1 maps obtained from subjects on different regions of white matter (WM) and gray matter (GM) on cSC, and WM, GM and deep GM on brain. T1 values were compared with those from previous brain or SC studies. Furthermore, the inter-session reproducibility of the technique was assessed for prospective clinical application on progressive degenerative diseases.

2 Materials & Methods

2.1 *Simulation*

Simulations mainly focused on CNR and sensitivity to B_1^+, considering a 3D isotropic acquisition allowing to cover both brain and cSC (sagittal orientation preferred here) with a sub-millimetric resolution (0.9 mm here). Simulation were performed by varying the main parameters that determine the unique relationship between the UNI image and the T_1 map [12]. The MP2RAGE repetition time (MP2RAGE TR) was varied between 4000 and 6000 ms using a 250 ms step. The number of excitations per RAGE module was set to 176 (required value to cover the brain width, using a 6/8 partial fourier) and the TR was kept fixed at 6 ms. The first and second inversion times (TI1/TI2) were then varied in steps of 50 ms. First and second RAGE flip angles (α_1/α_2) varied from 3° to 15°. The five main parameters which are MP2RAGE TR, TI1/TI2 and α_1/α_2 were varied and CNR and signal variation with B_1^+ inhomogeneity were investigated at the same time.

For that purpose, a broad range of T_1 values (between 500 ms and 3000 ms) was consequently considered for the simulations in order to cover values observed in both cord and brain. The T_1 values set for SC WM and GM were 880 ms and 970 ms according to Smith et al. [29], and for the Cerebrospinal Fluid (CSF), an upper T_1 of 3000 ms was considered for the simulation based on previous data acquired. The range of T_1 values also covered T_1s observed on the brain (810 ms for WM, 1350 ms for GM, 1250 ms for Nucleus caudate and 1130 ms for Putamen [12]).

The CNR per unit time between two tissues was calculated based on the formulas described in Marques et al. [12] as:

$$CNR_{tissue1VStissue2} = \frac{MP2RAGE_{tissue1} - MP2RAGE_{tissue2}}{\sqrt{\sigma_{tissue1}^2 + \sigma_{tissue2}^2}} . \frac{1}{\sqrt{MP2RAGE_{TR}}} \quad (1),$$

with

$$\sigma_{tissue} = a\sqrt{\frac{(GRE_{TI1}{}^2 - GRE_{TI2}{}^2)^2}{(GRE_{TI1}{}^2 + GRE_{TI2}{}^2)^3}} \quad (2),$$

with $MP2RAGE_{tissue1}$ and $MP2RAGE_{tissue2}$ the UNI signal in tissue 1 and tissue 2 respectively, $\sigma_{tissue1}$ and $\sigma_{tissue2}$ the noise propagation in tissue 1 and tissue 2, respectively, GRE_{TI1} and GRE_{TI2} the volumes acquired at first and second inversion times (in each tissue) and "a" the magnitude of the noise. In the simulation, the noise was considered to be of the same magnitude in each tissue and therefore, for different protocols relative to each other, the term "a" was not considered anymore.

When optimizing the protocols, maximization of CNR was performed emphasizing on the WM/GM and WM/CSF on cSC, for which segmentation may be more problematic than in the brain, using a global CNR defined as:

$$CNR = CNR_{GMvsWM} . CNR_{WMvsCSF} \quad (3)$$

Finally, a B_1^+ map obtained and averaged from 3 healthy volunteers (same volunteers used later on for in-vivo experiments) was used to determine representative B_1^+ variations encountered in brain and cSC. As seen on Figure 1, in regions with the highest field inhomogeneities such as brainstem and cerebral cortex on brain, and C1 and C7 on the cord, a B_1^+ variation of ±20% can be observed and this value was subsequently used in the

simulation part. A T_1 estimation error of less than 10% was set as a criterion for this value and considered for cSC WM, GM and brain WM, GM, and deep GM.

Sets of parameters ((α_1/α_2, TI_1, TI_2, MP2RAGE TR) leading to a non-bijective behavior in lower and upper T_1 boundaries (500 ms and 3000 ms) were removed.

Figure 2 shows the simulated relationship between the UNI signal and the T_1 values in normal conditions and under ±20% B_1^+ variations for 4 different protocols. The first one (fig. 2a), with $TI1/TI2 = 800/3500\,ms; \alpha_1/\alpha_2 = 6/3\,; and\ MP2RAGE\ TR = 4750\,ms$, which was named Pr-max, provided the highest simulated CNR, at the expense of acquisition time (9.2 minutes). The second protocol (fig. 2b), $TI1/TI2 = 650/3150\,ms; \alpha_1/\alpha_2 = 5/3\,; MP2RAGE\ TR = 4000\,ms$ named Pr-BSC, provided a high simulated CNR (though 13% lower than in Pr-max), while allowing to cover brain and cSC in less than 8 minutes. The third and fourth protocols (fig. 2c & fig. 2d) were previously optimized for studying brain [13], [16], and SC [21], [22], independently. Figure 3 shows the derivative of the UNI signal in relation with different T_1s (in optimal B_1^+ condition) for each protocol. This figure shows the ability and performance of each protocol in tissue discrimination. Given its CNR and acquisition time, Pr-BSC was kept for subsequent in vivo studies

2.2 In-vivo experiment

Protocols Pr-BSC, Pr-SC and Pr-B were tested on healthy volunteers. Sequence parameters for each protocol are provided in table 1. Data were acquired on a 3T Siemens Verio scanner with 12-channel head and 4-channel neck coils (Siemens Healthineers, Erlangen, Germany). Three healthy volunteers (27, 37, 45 years old, 1M/2F) were scanned in three separate sessions with each protocol, to assess the inter-session reproducibility of each sequence. The local ethics committee of our institution approved all experimental procedures of the study, and written informed consent was obtained from each volunteer.

A B_1^+ map acquired using a preconditioning RF pulse with turboFLASH readout[30] with a resolution of 5 mm isotropic was additionally used to correct T_1 maps.

The complete post-processing pipeline used to extract metrics in different brain and cSC ROIs is shown in Figure 4. The first step consisted of the B_1^+ correction of the individual quantitative T_1 maps using a 3D look-up table (LUT) providing relationship between UNI and T_1 values in the presence of B_1^+ variation. Then on brain, after anterior-posterior commissure (AC-PC) alignment of images [31], the UNI-denoised image (provided by the scanner) was used for segmentation of GM and WM with SPM 12 (https://fil.ion.ucl.ac.uk/spm) "New segment" tool [32] and for segmentation of deep GM structures (including Nucleus caudate, Putamen and Thalamus) with FSL-FIRST (https://fsl.fmrib.ox.ac.uk/) [33]. Data were then registered to MNI-152 atlas using SyN-ANTS [34] and divided into different lobes of frontal, parietal, temporal and occipital by ICBM MNI-152 lobes atlas [35], [36]. On SC, segmentation of the cord was first performed using the spinal cord toolbox (SCT [37]), then the T_1 map was registered to PAM50 template, which is an unbiased multimodal MRI template of the SC and brainstem [38]. For T_1 quantification, PAM50 masks including gray matter anterior and intermediate, white matter corticospinal, posterior sensory, lateral sensory and rubro/reticulospinal tracts were warped back into the subject space.

The mean and standard deviation (SD) of the corrected T_1 quantitative map was calculated in each brain and cSC ROI for each session and subject. The SD is reported for each ROI (in-ROI SD), between different sessions for each subject (inter-session SD) and between different subjects (inter-subject SD). Reproducibility for each protocol was assessed using the coefficient of variation (COV), defined as mean/inter-session SD. Statistical analyses were performed by JMP, Version 9 (SAS Institute Inc., Cary, NC).

3 Results

Figure 5 shows a representation of the UNI-denoised image on one subject for Pr-BSC and Pr-B on brain and Pr-BSC and Pr-SC on SC. The sub-millimetric resolution of the technique allowed us to capture different structures of brain and cSC.

To transpose the results of simulation, the CNR per unit time for in-vivo data was calculated from the previously defined formulae (1), using the average and the SD of the UNI signal in a tissue as $MP2RAGE_{tissue}$ and σ_{tissue}, respectively. For the sake of simplicity, a global CNR for the whole GM/WM in brain for all protocols, and GM/WM and WM/CSF on cSC for Pr-SC and Pr-BSC on each subject was calculated, and the results are summarized in table 2. The optimized Pr-BSC provided higher CNR for each subject in both brain and cSC.

Figure 6 shows the T_1 comparison between Pr-BSC and Pr-SC on cSC (fig. 6a) and Pr-BSC and Pr-B on brain (fig. 6b). An excellent agreement was seen on brain with a Pearson correlation coefficient of 0.99 and a Bias±LOA (Limits of Agreement)=4.0±28.1 ms. On SC, this correlation was found equal to 0.88 with a Bias±LOA=25.1±38.8 ms. It should be noted that the bias on SC is lower than the mean in-ROI SD observed in cSC (around 39 ms).

The average T_1 values found with Pr-BSC on different regions of WM and GM on brain and cSC are summarized in table 3, together with values reported previously in the literature. The mean T_1 values observed with our optimized Pr-BSC in brain WM, GM and deep GM were 792±27 ms, 1339±139 ms and 1136±88ms, respectively. In the cSC, the values for WM corticospinal (CST), posterior sensory (PST), lateral sensory (LST) and rubrospinal & reticulospinal (RST) tracts were 902±41 ms, 920±35 ms, 903±46 ms, 891±41 ms, respectively, and 954±32ms for anterior & intermediate GM. No statistically significant differences were observed between different cervical levels. Inter-subject, in-ROI and inter-session SD values are also reported. In average, the values were found in the order of 2.65%, 6.24% and 0.67%.
Finally, the inter-session COV, calculated for each ROI, is detailed in Figure 7. All three protocols demonstrated a great reproducibility in average (see fig. 7a), with the COV being slightly better for Pr-BSC (not statistically significant). The highest COV (lowest reproducibility) was lower than 3% and observed at the C7 SC level (fig. 7e).

4 Discussion

In this work, a simulation-based parameter optimization led to the identification of a high resolution T_1 mapping MP2RAGE protocol with high contrasted UNI images covering both brain and whole cSC in a single acquisition.

The optimized Pr-BSC showed excellent agreement with the T_1 values obtained with the standard brain protocol (Pr-B) in all ROIs [13], [16]. On cSC, a small bias (25 ms,

representing 2.8% of the mean T1) was observed as compared to the reference protocol [21], which represents less than the average cSC in-ROI SD and was therefore not further investigated.

The optimized Pr-BSC also demonstrated high inter-session reproducibility (with the lowest COV observed on brain WM and highest on the C7 spinal level), hence opening promising perspectives for longitudinal follow-up studies.

It should be mentioned that Pr-SC originally proposed for the cord by Rasoanandrianina et al. [21] incidentally covered brain, however cerebral T_1 values were not investigated in their initial study. Here, a bias in the order of 20 ms (which is lower than in-ROI SD) was observed when comparing Pr-SC to Pr-B, which was not further analyzed as our purpose was to benefit from increased CNR. However, this indicates that Pr-SC could also be used for brain investigation although not optimal, if subject to further investigation of potential bias in T_1 estimation. Reciprocally, Pr-B partially covers the cSC (down to C4 level), however quantification was not considered since whole cervical cord was required here. Brainstem and cerebellum are also fully quantifiable with the MR protocols used in this study, subject to additional postprocessing optimization not considered here.

Pr-BSC also provides an increased CNR as compared to Pr-B, which was initially optimized for both CNR and B_1^+ immunity. Here, CNR gain optimization made for Pr-BSC comes at an expense of B_1^+ immunity and further necessitates a B_1^+ correction strategy (as previously proposed by Massire et al. [20]). The different coil set ups (12+4 channel head and neck here, as compared to optimal 32 channel in the original study [13], [16]) may also have slightly influenced the results..

Finally, this feasibility study was performed on a small number of volunteers in order to test and validate the optimized Pr-BSC, to investigate the reproducibility for longitudinal follow-ups, and to assess the performance of the automatic post-processing pipeline. Future studies should now focus on the sensitivity of the technique to detect disease progression, to assess therapeutical efficacy, inter-site reproducibility in the perspective of multi-centric studies and to provide representative normative values. The recently proposed compressed sensing (CS-MP2RAGE) [39] technique could be considered to further reduce the acquisition time and make it even more suitable for clinical practice.

5 Conclusion

This work proposes an optimized protocol dedicated to sub-millimetric simultaneous brain and cSC T_1 MP2RAGE mapping at 3T, compatible with clinical scan time.

The protocol showed excellent agreement with previously proposed protocols for brain and cSC independently. It also demonstrated high inter-scan reproducibility, hence opening up great perspectives for longitudinal clinical applications, especially in the context of neurodegenerative (MS, ALS) diseases and SC injuries.

Acknowledgement:

This work was performed within a laboratory member of France Life Imaging network (grant ANR-11-INBS-0006) and was supported by the Institut Carnot Star, the ARSEP Fundation (Fondation pour l'Aide à la Recherche sur la Sclérose en Plaques) and the CNRS (Centre National de la Recherche Scientifique). The project also received funding from the European Union's Horizon 2020 research and innovation program under the Marie Skłodowska-Curie grant agreement No713750, with the financial support of the Regional Council of Provence-Alpes-Côte d'Azur and A*MIDEX (n° ANR-11-IDEX-0001-02), funded by the Investissements d'Avenir project funded by the French Government, managed by the French National Research Agency (ANR).
The authors would like to thank T. Kober from Siemens Healthcare for MP2RAGE sequence support, A. Massire for T_1-postprocessing code support, as well as V. Gimenez, C. Costes and L. Pini for study logistics.

References

[1] E. M. Haacke *et al.*, "Imaging iron stores in the brain using magnetic resonance imaging," *Magn. Reson. Imaging*, vol. 23, no. 1, pp. 1–25, 2005.

[2] J. Sian-Hülsmann, S. Mandel, M. B. H. Youdim, and P. Riederer, "The relevance of iron in the pathogenesis of Parkinson's disease," *J. Neurochem.*, vol. 118, no. 6, pp. 939–957, 2011.

[3] L. Nürnberger *et al.*, "Longitudinal changes of cortical microstructure in Parkinson's disease assessed with T1 relaxometry," *NeuroImage Clin.*, vol. 13, pp. 405–414, 2017.

[4] F. Paul, "Pathology and MRI: exploring cognitive impairment in MS," *Acta Neurol. Scand.*, vol. 134, no. July, pp. 24–33, 2016.

[5] M. D. Steenwijk *et al.*, "High-resolution T1-relaxation time mapping displays subtle, clinically relevant, gray matter damage in long-standing multiple sclerosis," *Mult. Scler.*, vol. 22, no. 10, pp. 1279–1288, 2016.

[6] H. L. Margaret Cheng, N. Stikov, N. R. Ghugre, and G. A. Wright, "Practical medical applications of quantitative MR relaxometry," *J. Magn. Reson. Imaging*, vol. 36, no. 4, pp. 805–824, 2012.

[7] P. A. Gowland and M. O. Leach, "A simple method for the restoration of signal polarity in multi-image inversion recovery sequences for measuring T1," *Magn. Reson. Med.*, vol. 18, no. 1, pp. 224–231, 1991.

[8] P. Gowland and P. Mansfield, "Accurate measurement of T1 in vivo in less than 3 seconds using echo-planar imaging," *Magn. Reson. Med.*, vol. 30, no. 3, pp. 351–354, 1993.

[9] D. Holland, J. M. Kuperman, and A. M. Dale, "Efficient correction of inhomogeneous static magnetic field-induced distortion in Echo Planar Imaging," *Neuroimage*, vol. 50, no. 1, pp. 175–183, 2010.

[10] S. C. L. Deoni, B. K. Rutt, and T. M. Peters, "Rapid combined T1 and T2 mapping using gradient recalled acquisition in the steady state," *Magn. Reson. Med.*, vol. 49, no. 3, pp. 515–526, 2003.

[11] R. Heule, C. Ganter, and O. Bieri, "Variable flip angle T1 mapping in the human brain with reduced t2 sensitivity using fast radiofrequency-spoiled gradient echo imaging," *Magn. Reson. Med.*, vol. 75, no. 4, pp. 1413–1422, 2016.

[12] J. P. Marques, T. Kober, G. Krueger, W. van der Zwaag, P. F. Van de Moortele, and R. Gruetter, "MP2RAGE, a self bias-field corrected sequence for improved segmentation and T1-mapping at high field," *Neuroimage*, vol. 49, no. 2, pp. 1271–1281, 2010.

[13] T. Kober *et al.*, "MP2RAGE multiple sclerosis magnetic resonance imaging at 3 T," *Invest. Radiol.*, vol. 47, no. 6, pp. 346–352, 2012.

[14] G. Okubo *et al.*, "MP2RAGE for deep gray matter measurement of the brain: A comparative study with MPRAGE," *J. Magn. Reson. Imaging*, vol. 43, no. 1, pp. 55–62, 2016.

[15] J. P. Marques and R. Gruetter, "New Developments and Applications of the MP2RAGE Sequence - Focusing the Contrast and High Spatial Resolution R1 Mapping," *PLoS One*, vol. 8, no. 7, p. e69294, 2013.

[16] S. Simioni *et al.*, "MP2RAGE provides new clinically-compatible correlates of mild cognitive deficits in relapsing-remitting multiple sclerosis," *J. Neurol.*, vol. 261, no. 8, pp. 1606–1613, 2014.

[17] M. Filippi *et al.*, "Intracortical lesions: Relevance for new MRI diagnostic criteria for

multiple sclerosis," *Neurology*, vol. 75, no. 22, pp. 1988–1994, 2010.
[18] B. Simon *et al.*, "Improved in vivo detection of cortical lesions in multiple sclerosis using double inversion recovery MR imaging at 3 Tesla," *Eur. Radiol.*, vol. 20, no. 7, pp. 1675–1683, 2010.
[19] B. Moraal *et al.*, "Multi-contrast, isotropic, single-slab 3D MR imaging in multiple sclerosis," *Eur. Radiol.*, vol. 18, no. 10, pp. 2311–2320, 2008.
[20] A. Massire, M. Taso, P. Besson, M. Guye, J. P. Ranjeva, and V. Callot, "High-resolution multi-parametric quantitative magnetic resonance imaging of the human cervical spinal cord at 7T," *Neuroimage*, vol. 143, pp. 58–69, 2016.
[21] H. Rasoanandrianina *et al.*, "Regional T1 mapping of the whole cervical spinal cord using an optimized MP2RAGE sequence," *NMR Biomed.*, vol. 32, no. 11, pp. 1–17, 2019.
[22] S. Demortière, P. Lehmann, J. Pelletier, B. Audoin, and V. Callot, "Improved cervical cord lesion detection with 3D-MP2RAGE sequence in patients with multiple sclerosis," *Am. J. Neuroradiol.*, vol. 41, no. 6, pp. 1131–1134, 2020.
[23] P. Freund *et al.*, "Embodied neurology: An integrative framework for neurological disorders," *Brain*, vol. 139, no. 6, pp. 1855–1861, 2016.
[24] J. Cohen-Adad *et al.*, "BOLD signal responses to controlled hypercapnia in human spinal cord," *Neuroimage*, vol. 50, no. 3, pp. 1074–1084, 2010.
[25] J. Finsterbusch, C. Sprenger, and C. Büchel, "Combined T2*-weighted measurements of the human brain and cervical spinal cord with a dynamic shim update," *Neuroimage*, vol. 79, pp. 153–161, 2013.
[26] H. Islam, C. S. W. Law, K. A. Weber, S. C. Mackey, and G. H. Glover, "Dynamic per slice shimming for simultaneous brain and spinal cord fMRI," *Magn. Reson. Med.*, vol. 81, no. 2, pp. 825–838, 2019.
[27] M. Azzarito *et al.*, "Simultaneous voxel-wise analysis of brain and spinal cord morphometry and microstructure within the SPM framework," *Hum. Brain Mapp.*, no. January, pp. 1–13, 2020.
[28] K. R. O'Brien *et al.*, "Robust T1-weighted structural brain imaging and morphometry at 7T using MP2RAGE," *PLoS One*, vol. 9, no. 6, 2014.
[29] S. A. Smith, R. A. E. Edden, J. A. D. Farrell, P. B. Barker, and P. C. M. Van Zijl, "Measurement of T1 and T2 in the cervical spinal cord at 3 Tesla," *Magn. Reson. Med.*, vol. 60, no. 1, pp. 213–219, 2008.
[30] S. Chung, D. Kim, E. Breton, and L. Axel, "Rapid B1+ mapping using a preconditioning RF pulse with turboFLASH readout," *Magn. Reson. Med.*, vol. 64, no. 2, pp. 439–446, 2010.
[31] M. F. Glasser *et al.*, "The minimal preprocessing pipelines for the Human Connectome Project," *Neuroimage*, vol. 80, pp. 105–124, 2013.
[32] J. Ashburner and K. J. Friston, "Unified segmentation," *Neuroimage*, vol. 26, no. 3, pp. 839–851, 2005.
[33] B. Patenaude, S. M. Smith, D. N. Kennedy, and M. Jenkinson, "A Bayesian model of shape and appearance for subcortical brain segmentation," *Neuroimage*, vol. 56, no. 3, pp. 907–922, 2011.
[34] B. B. Avants, N. Tustison, and G. Song, "Advanced normalization tools (ANTS)," *Insight j*, vol. 2, no. 365, pp. 1–35, 2009.
[35] V. Fonov, A. Evans, R. McKinstry, C. Almli, and D. Collins, "Unbiased nonlinear average age-appropriate brain templates from birth to adulthood," *Neuroimage*, vol. 47, p.

S102, Jul. 2009.
[36] V. Fonov, A. C. Evans, K. Botteron, C. R. Almli, R. C. McKinstry, and D. L. Collins, "Unbiased average age-appropriate atlases for pediatric studies," *Neuroimage*, vol. 54, no. 1, pp. 313–327, 2011.
[37] B. De Leener *et al.*, "SCT: Spinal Cord Toolbox, an open-source software for processing spinal cord MRI data," *Neuroimage*, vol. 145, no. October 2016, pp. 24–43, 2017.
[38] B. De Leener, V. S. Fonov, D. L. Collins, V. Callot, N. Stikov, and J. Cohen-Adad, "PAM50: Unbiased multimodal template of the brainstem and spinal cord aligned with the ICBM152 space," *Neuroimage*, vol. 165, no. July 2017, pp. 170–179, 2018.
[39] E. Mussard, T. Hilbert, C. Forman, R. Meuli, J. P. Thiran, and T. Kober, "Accelerated MP2RAGE imaging using Cartesian phyllotaxis readout and compressed sensing reconstruction," *Magn. Reson. Med.*, vol. 84, no. 4, pp. 1881–1894, 2020.
[40] P. J. Wright *et al.*, "Water proton T1 measurements in brain tissue at 7, 3, and 1.5T using IR-EPI, IR-TSE, and MPRAGE: Results and optimization," *Magn. Reson. Mater. Physics, Biol. Med.*, vol. 21, no. 1–2, pp. 121–130, 2008.
[41] M. Battiston *et al.*, "Fast and reproducible in vivo T1 mapping of the human cervical spinal cord," *Magn. Reson. Med.*, vol. 79, no. 4, pp. 2142–2148, 2018.

Tables

Table 1 : Parameters used in each protocol for brain and spinal cord imaging.

	TI1/TI2	α_1/α_2	MP2RAGE TR / Total acq. time	FOV	Resolution	PAT factor
Pr-BSC (this study)	650/3150 ms	5/3	4000 ms/ 7.8 min	315x262 mm	0.9 mm iso	2
Pr-SC [21], [22]	600/2000 ms	4/5	4000 ms/ 7.8 min	315x262 mm	0.9 mm iso	2
Pr-B [13], [16]	700/2500 ms	4/5	5000 ms/ 8.4 min	256x240 mm	1 mm iso	3

Table 2: CNR per unit time (which takes into account the MP2RAGE TR) calculated on each subject for GM/WM on brain and cSC. The CNR GM/WM on brain was also calculated for Pr-SC since this protocol allowed covering the brain. On the other hand, Pr-B could not cover the entire cervical cord so CNR for SC GM/WM was not calculated in that case. The optimized Pr-BSC provided the highest CNR on each subject and on average for brain and cSC, separately. Please note that the coil set-up used here (12+4 channels for brain and cSC) is different from the 32 channel head-coil used in previous papers[13], [16] *and might not be optimal for Pr-B with regards to CNR. However, since the CNR reported in* [13] *are reported as normalized by CNR of FLAIR images, a direct comparison is not possible here.*

	CNR for brain GM/WM			CNR for SC GM/WM		CNR for SC WM/CSF	
	Pr-BSC	Pr-B	Pr-SC	**Pr-BSC**	Pr-SC	**Pr-BSC**	Pr-SC
Sub 1	**1.75**	1.45	1.60	**0.27**	0.23	**3.14**	2.50
Sub 2	**1.67**	1.46	1.61	**0.29**	0.27	**2.82**	2.64
Sub 3	**1.57**	1.46	1.51	**0.29**	0.28	**3.90**	3.51
Mean	**1.66±0.09**	1.45±0.01	1.57±0.05	**0.28±0.01**	0.26±0.02	**3.28±0.55**	2.88±0.54

Table 3: Average T_1 values (in ms) obtained with Pr-BSC in this study on brain and SC and comparison with values reported in previous studies either on the brain or the cord. For this study, the standard deviations (in ms) are reported for inter-subject, in-ROI and inter-session (mean of the individual inter-session SD). The inter-session SD is the lowest SD in all regions (in this study), which shows a great robustness for the technique. For the other studies cited in the table, the SD represents the inter-subject variation. A good agreement with previously reported T_1 MP2RAGE values (Marques 2010[12], *Rasoanandrianina 2019*[21]*) was observed. CST: Corticospinal Tracts, PST: Posterior Sensory Tracts, LST: Lateral Sensory Tracts, RST: Reticulo/Rubrospinal Tracts.*

Brain					
This study (mean±[inter-subject SD; ROI SD; inter-session SD])			Marques 2010 [12] (MP2RAGE)	Wright 2008 [40] (MPRAGE)	Okubo 2015 [14] (MP2RAGE)
WM	Frontal	787±[15;23;2]	810±30	840±50	-
	Parietal	794±[8;23;2]			
	Occipital	790±[10;30;2]			
	Temporal	797±[8;34;2]			
GM	Frontal	1312±[57;139;10]	1350±50	1610±100	
	Parietal	1322±[50;136;11]			
	Occipital	1318±[31;139;9]			
	Temporal	1407±[50;135;10]			
Deep GM	Caudate	1206±[18;65;6]	1250±70	1390±50	1217±30
	Putamen	1151±[51;84;4]	1130±70	1330±70	1095±31
	Thalamus	1053±[22;115;7]	1080±70	-	1077±30
SC					
This study (mean±[inter-subject SD; ROI SD; inter-session SD])			Rasoanandrianina 2019 [14] (MP2RAGE)	Smith 2008 [29] (IR)	Battiston 2017 [41] (IR ZOOM-EPI)
WM	CST	902±[18;41;10]	877±35	876±27	-
	PST	920±[28;35;10]	920±37		-
	LST	903±[34;46;9]	-		1110±83
	RST	891±[25;41;9]	-		
GM	Anterior & Intermediate	954±[35;32;10]	934±33	973±33	1136±90

Figures

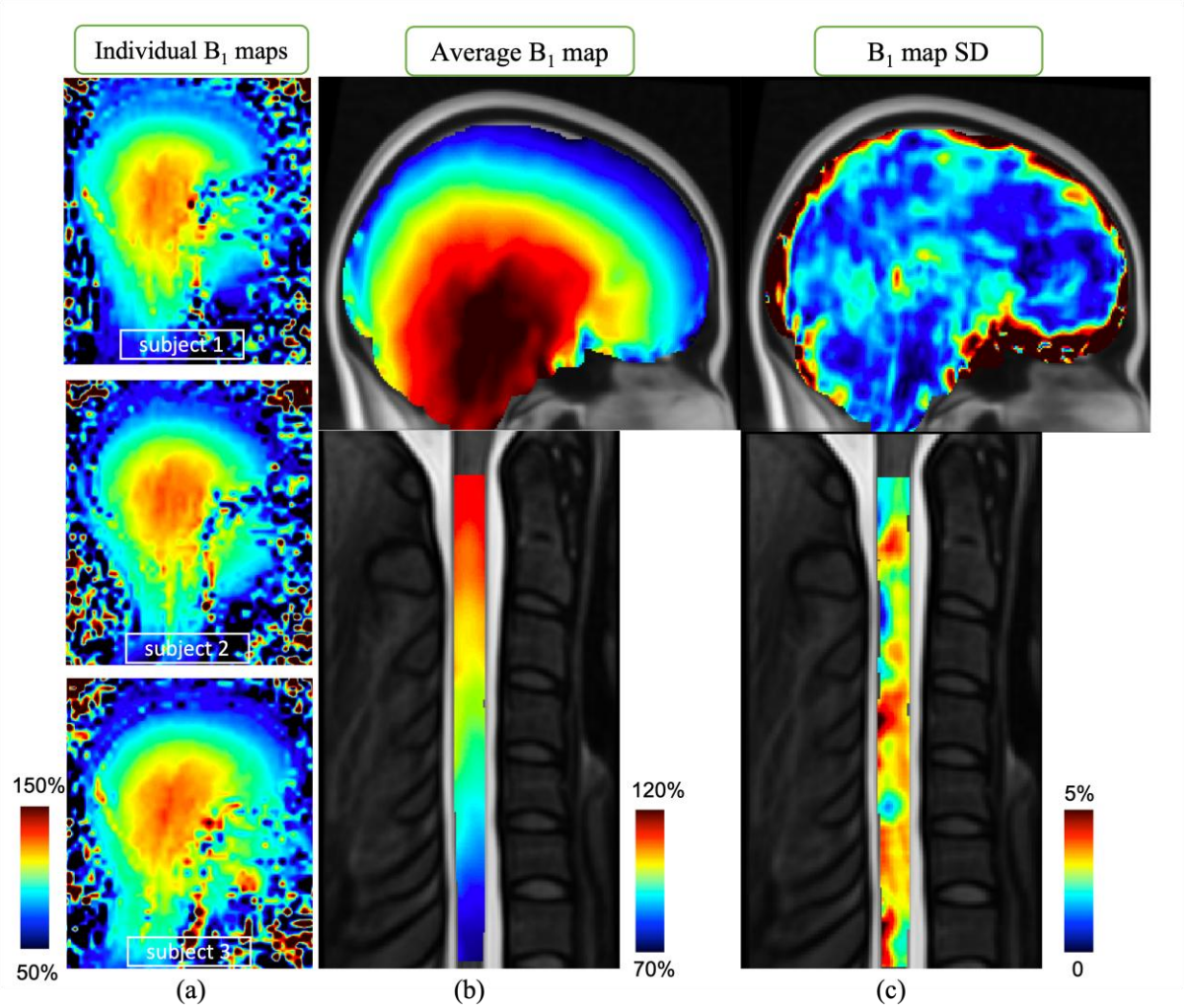

Figure 1: (a) Individual B_1^+ maps acquired with preconditioning RF pulse with TurboFLASH Readout [30] *on 3 healthy subjects. (b) Mean and (c) standard deviation of B_1^+ maps over 3 healthy subjects, presented in the ICBM MNI-152* [35], [36] *and PAM50* [38] *spaces. It can be observed in (b) that the highest B_1^+ field inhomogeneities can be observed in brainstem and cerebral cortex on brain, and C1 and C7 on the cord and in these regions, a B_1^+ variation of ±20% can be observed. In (c) the inter-subject variation of B_1^+ is less than 5%; however, it should be noted that with different morphologies (larger neck or longer spine) this variation could be increased.*

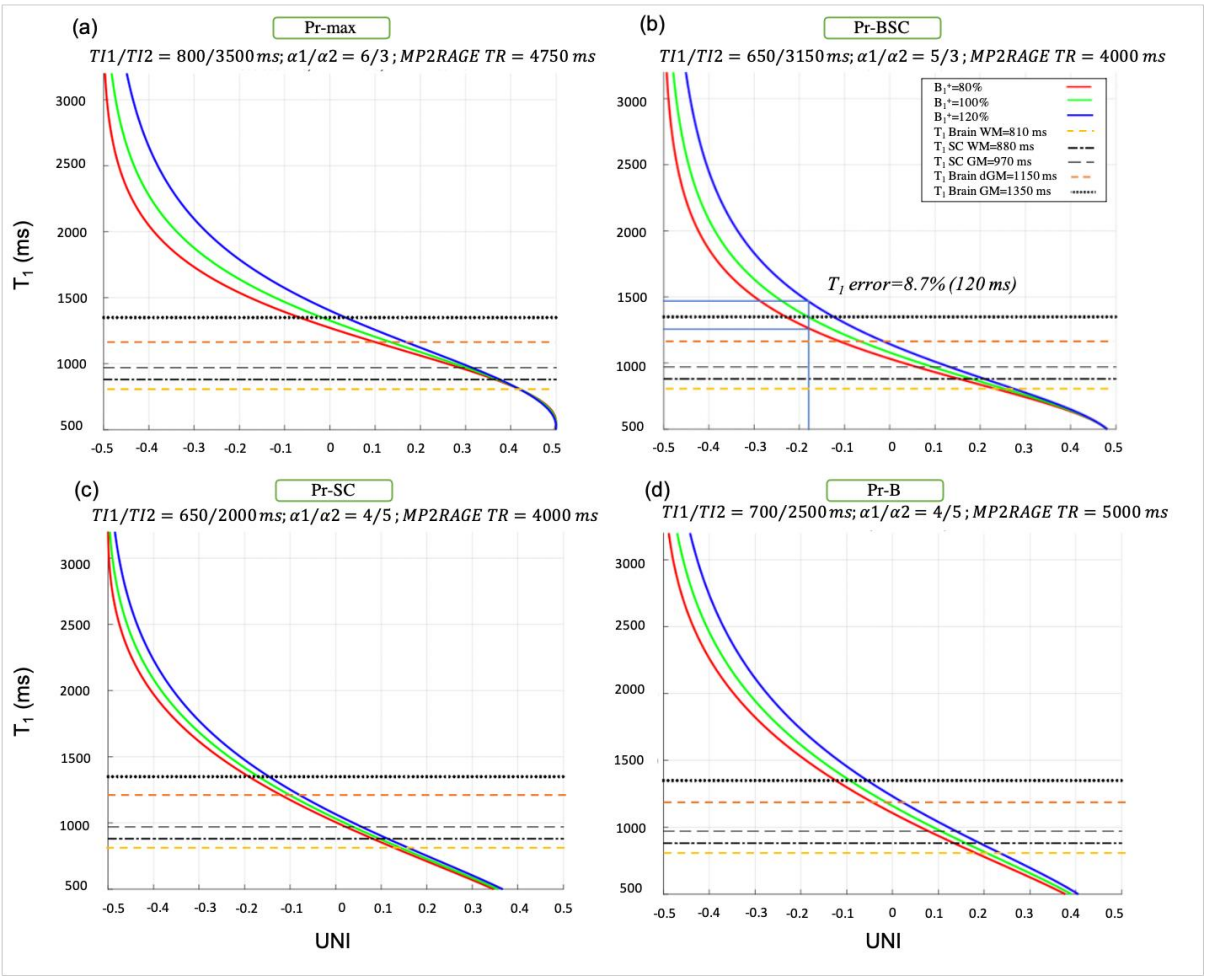

Figure 2: (a-d) Relationships between UNI signal and estimated T_1 values in normal condition (green curve) and with ±20% B_1^+ variation (blue/red curves). (a) The protocol Pr-max, derived from the CNR simulation optimization process, provides the highest CNR but at the expense of acquisition time (9.2 minutes). (b) The protocol Pr-BSC provides a high CNR, while allowing to cover brain and cSC in 7.8 minutes. Despite optimization, it should be noted that a ±20% B_1^+ variation for a T_1 of 1350 (brain GM) for instance, leads to an estimation error of 8.7% in T_1 determination (i.e. up to 120 ms), which imposes the necessity for B_1^+ correction for accurate T_1 mapping. Such variations for lower T_1 s are less as can be seen and for example, for T_1s of less than 1000 ms, we can expect an estimation error of less than 5%. Pr-SC and Pr-B correspond to previously optimized protocols for studying (c) SC [21], [22], *and (d) brain* [13], [16], *independently, with acquisition time of 7.8 minutes and 8.4 minutes, respectively.*

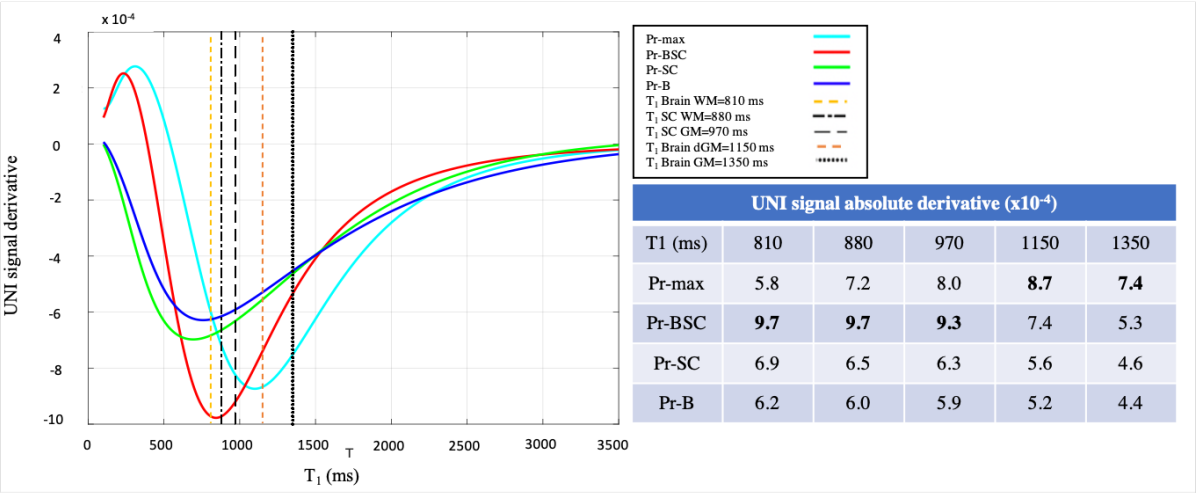

UNI signal absolute derivative (x10^{-4})					
T1 (ms)	810	880	970	1150	1350
Pr-max	5.8	7.2	8.0	**8.7**	**7.4**
Pr-BSC	**9.7**	**9.7**	**9.3**	7.4	5.3
Pr-SC	6.9	6.5	6.3	5.6	4.6
Pr-B	6.2	6.0	5.9	5.2	4.4

Figure 3: (left) Derivative of the UNI signal along T_1 values (slope of the graphs in figure 2) ; this graph provides indications on the specificity of each protocol and their performance in discriminating between different tissues. The table (right) summarizes the absolute of that signal derivative for different T_1s found in brain and cSC tissues. For T_1s < 1040 ms, Pr-BSC shows the highest (absolute) values and for T_1s > 1040 ms the Pr-max shows the highest values. For the whole range, Pr-BSC shows higher values than Pr-SC and Pr-B, i.e. higher ability to discriminate between different tissues. It should be noted that this advantage comes at the expense of a lower B_1^+ immunity which necessitates the implementation of a B_1^+ correction strategy to avoid T_1 estimation biases.

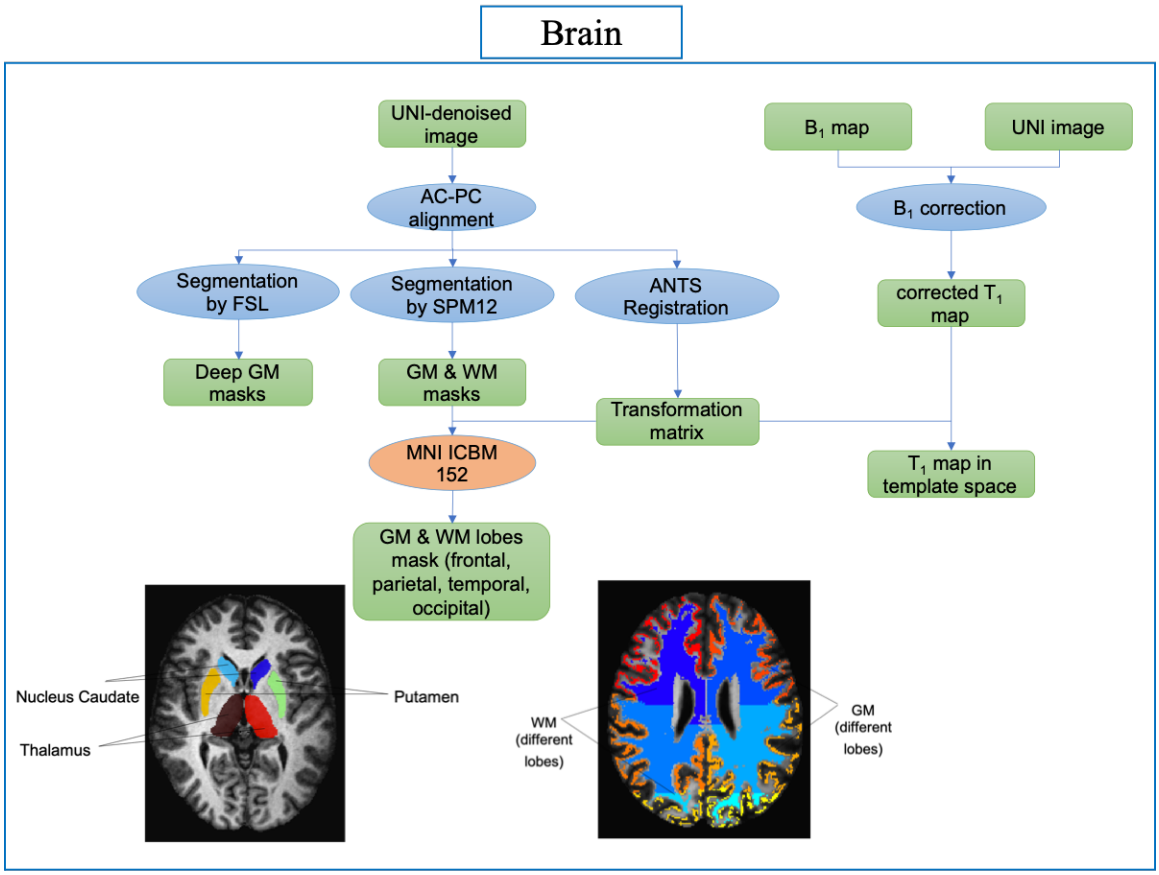

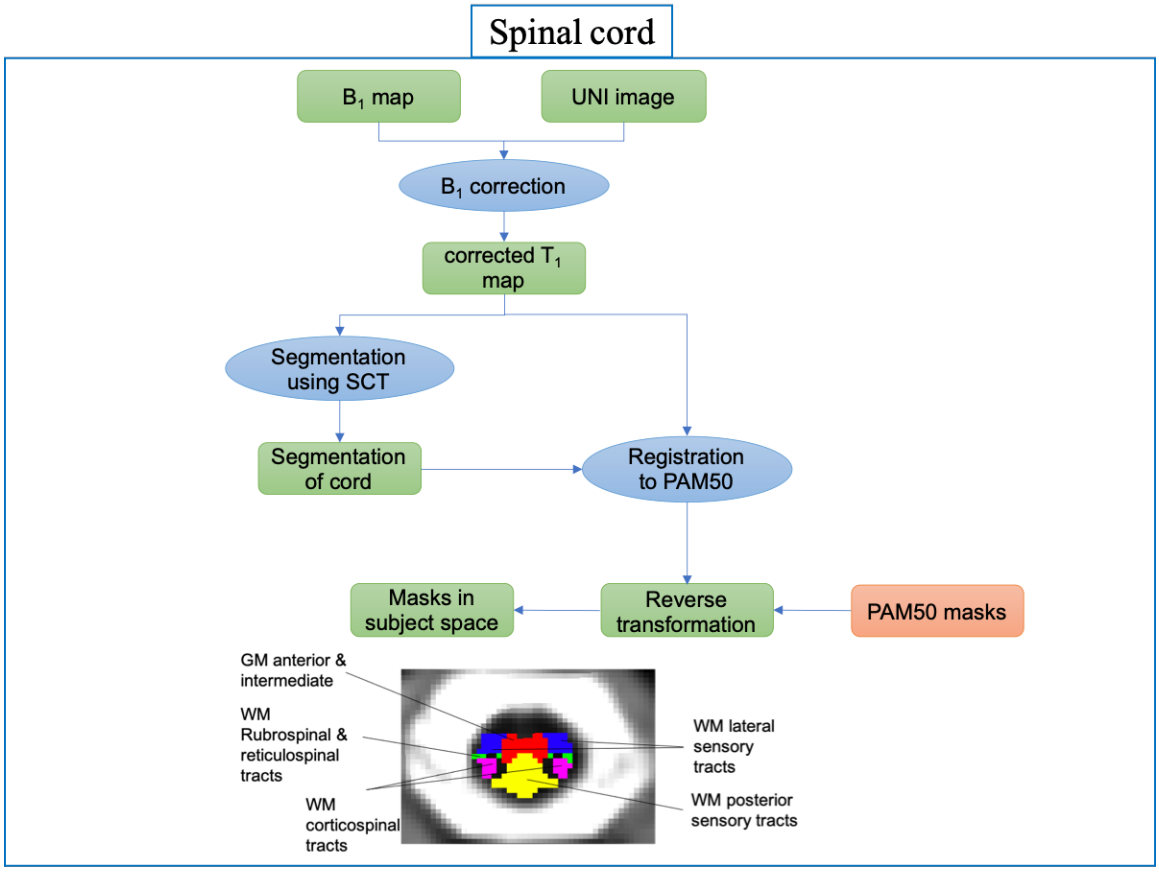

Figure 4: Post-processing steps for brain and cSC, with indication of the main regions of interest.

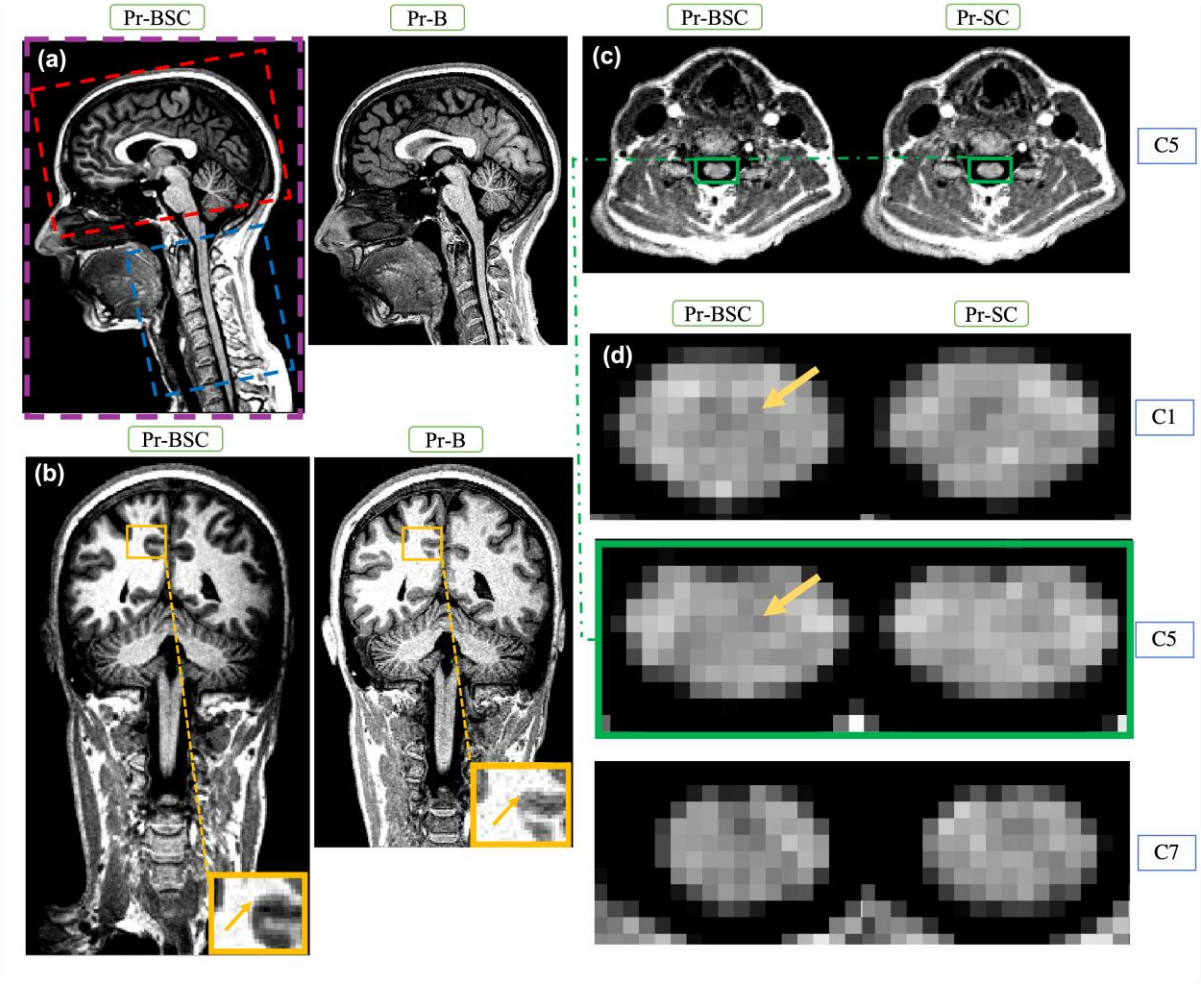

Figure 5: (a) Representation of UNI-denoised image (no unit) for Pr-BSC (FOV 315x262 mm^2) and Pr-B (FOV 256x240 mm^2) on brain in sagittal and (b) coronal views. (c) Representation of UNI-denoised image for Pr-BSC and Pr-SC in the axial plane at the C5 level, and (d) with a zoomed view along the cervical SC (C1, C5 and C7). In (a) the red box represents the volume of interest in previous brain studies [13], [16], *the blue box represents the volume of interest in previous cSC studies* [21], [22] *and the purple box shows how Pr-BSC covers both brain and cSC in a single acquisition. Moreover, Pr-BSC provided a nice delineation between different structures of brain (yellow arrows) and on cSC, the yellow arrows demonstrate the signal difference between GM and WM.*

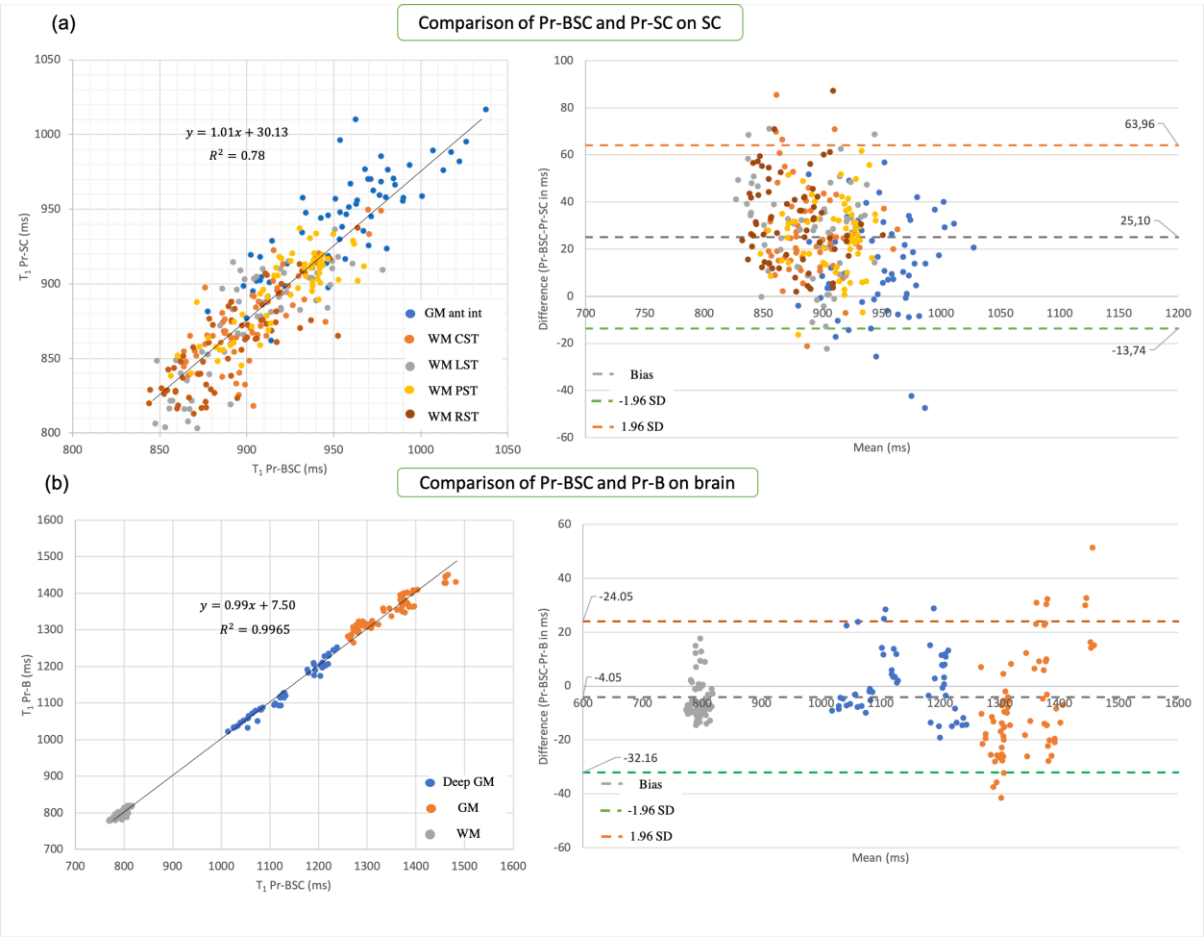

Figure 6: (a) comparison between Pr-BSC and Pr-SC on different ROIs of cSC; (b) comparison between Pr-BSC and Pr-B on brain (all subjects and sessions considered). The graphs on the left show the correlation graphs, with T1_Pr-BSC and T1_Pr-SC having a Pearson correlation coefficient of 0.88 (R^2=0.78) and T1_Pr-BSC and T1_Pr-B a correlation of 0.99 (R^2=0.99). On the right, the Bland-Altman plots can be observed along with the biases and Limits of Disagreement (LOA). The Bias±LOA between Pr-BSC and Pr-SC on SC is 25.1±38.8 ms and for Pr-BSC and Pr-B is 4.0±28.1 ms.

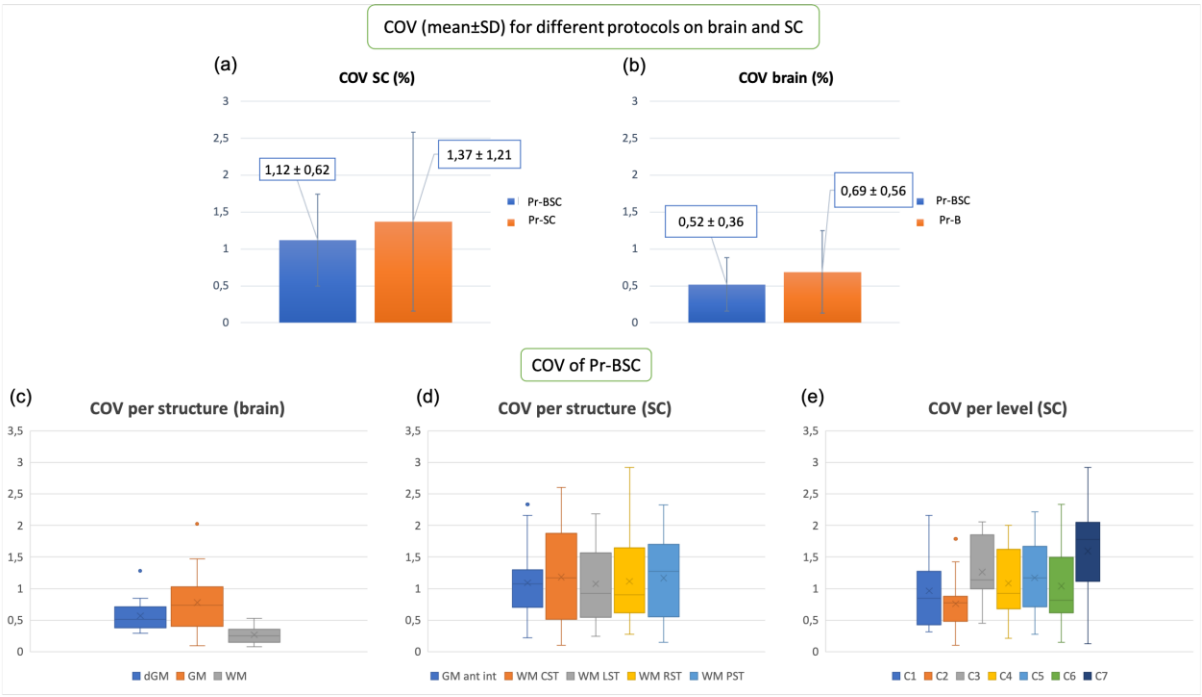

Figure 7: (a,b) average inter-session COV (for all ROIs and subjects). Optimized Pr-BSC showed a slightly better (non-statistically significant) reproducibility than the other two; however, all three protocols perform very well with regards to reproducibility. On bottom, box and Whisker plots demonstrating COV observed with Pr-BSC in the brain (c), the cord (d) and per SC levels (e). The boxplot bars represent the minimum, the first quartile (25%), the median, the mean (shown with X mark), the third quartile (75%) and the maximum from bottom to top, respectively. The highest COV (lowest reproducibility) was observed on the C7 level of SC (for one subject and session) and was lower than 3%.